A genetic interaction map of cell cycle regulators

Maximilian Billmann[a,†], Thomas Horn[a,†], Bernd Fischer[b,c], Thomas Sandmann[a], Wolfgang Huber[b], and Michael Boutros[a,*]

[a]Division of Signaling and Functional Genomics, German Cancer Research Center, and Department of Cell and Molecular Biology, Heidelberg University, 69120 Heidelberg, Germany; [b]Genome Biology Unit, EMBL, 69118 Heidelberg, Germany; [c]Computational Genome Biology, German Cancer Research Center, 69120 Heidelberg, Germany

ABSTRACT **Cell-based RNA interference (RNAi) is a powerful approach to screen for modulators of many cellular processes. However, resulting candidate gene lists from cell-based assays comprise diverse effectors, both direct and indirect, and further dissecting their functions can be challenging. Here we screened a genome-wide RNAi library for modulators of mitosis and cytokinesis in *Drosophila* S2 cells. The screen identified many previously known genes as well as modulators that have previously not been connected to cell cycle control. We then characterized ~300 candidate modifiers further by genetic interaction analysis using double RNAi and a multiparametric, imaging-based assay. We found that analyzing cell cycle–relevant phenotypes increased the sensitivity for associating novel gene function. Genetic interaction maps based on mitotic index and nuclear size grouped candidates into known regulatory complexes of mitosis or cytokinesis, respectively, and predicted previously uncharacterized components of known processes. For example, we confirmed a role for the *Drosophila* CCR4 mRNA processing complex component *l(2)NC136* during the mitotic exit. Our results show that the combination of genome-scale RNAi screening and genetic interaction analysis using process-directed phenotypes provides a powerful two-step approach to assigning components to specific pathways and complexes.**

Monitoring Editor
Mark J. Solomon
Yale University

Received: Jul 7, 2015
Revised: Feb 9, 2016
Accepted: Feb 10, 2016

INTRODUCTION

Large-scale genetic screens have identified components of many biological processes in a broad spectrum of organisms (Patton and Zon, 2001; Jorgensen and Mango, 2002; St Johnston, 2002; Boutros and Ahringer, 2008). Such experiments have considerably expanded our knowledge of regulatory complexes and pathways. In recent years, classical genetic screens have been complemented by cell-based, loss-of-function experiments using RNA interference (RNAi; Kiger *et al.*, 2003; Boutros *et al.*, 2004; Carpenter and Sabatini, 2004; Kittler *et al.*, 2004; DasGupta *et al.*, 2005). Although screening technologies have made significant advances, moving from candidate "hit" lists to precise delineation of functional relationships has remained challenging. Prioritization of candidates for follow-up experimentation often relies on prior knowledge, leaving uncharacterized genes untouched. Therefore systematic and scalable secondary lines of screens are necessary to group candidates into functional categories, pathways, or complexes.

In yeast, systematic double-perturbation experiments, termed synthetic genetic arrays (SGAs), dSLAM, or E-MAPs (Pan *et al.*, 2004; Tong *et al.*, 2004; Schuldiner *et al.*, 2005), have been used to explore diverse biological processes and successfully identified previously undiscovered functional relationships (Tong *et al.*, 2004; Schuldiner *et al.*, 2005; Collins *et al.*, 2007). In both *Saccharomyces cerevisiae* and *Schizosaccharomyces pombe*, large collections of mutant alleles are available to generate maps of biological processes and compare their phylogenetic relationships (Dixon *et al.*, 2008; Roguev *et al.*, 2008; Jonikas *et al.*, 2009). The largest-scale

This article was published online ahead of print in MBoC in Press (http://www.molbiolcell.org/cgi/doi/10.1091/mbc.E15-07-0467) on February 24, 2016.

†These authors contributed equally.

M.Bi., T.H., T.S., W.H., and M.B. designed the experiments. M.Bi., T.H., and T.S. performed the experiments. M.Bi., T.H., and B.F. performed the analysis. M.Bi., T.H., B.F., T.S., W.H., and M.B. wrote the manuscript. All authors read and approved the manuscript for publication.

*Address correspondence to: Michael Boutros (m.boutros@dkfz.de).

Abbreviations used: APC/C, anaphase-promoting complex/cyclosome; CCT, cytosolic chaperonin–containing t-complex; CSI, connection specificity index; CSN, COP9-signalosome; FDR, false-discovery rate; GI, genetic interaction; PCC, Pearson correlation coefficient; pH3, phospho-Histone H3; RNAi, RNA interference; SAC, spindle assembly checkpoint; SGI, synthetic genetic interaction.

Supplemental Material can be found at:
http://www.molbiolcell.org/content/suppl/2016/02/15/mbc.E15-07-0467v1.DC1.html

synthetic genetic interaction study to date has generated genetic interaction profiles for ~75% of the yeast genome (Costanzo *et al.*, 2010). Although full-genome genetic interaction analysis has not yet been approached in metazoan cells, the concept of systematic codepletion and quantitative analysis has been applied in *Caenorhabditis elegans* (Lehner *et al.*, 2006; Tischler *et al.*, 2008), *Drosophila* cells (Bakal *et al.*, 2008; Horn *et al.*, 2011; Fischer *et al.*, 2015), and mouse (Roguev *et al.*, 2013) and human (Laufer *et al.*, 2013; Wang *et al.*, 2014) cell lines.

Here we describe a two-step approach that first prioritizes genes by genome-wide screening for subsequent medium-scale, imaging-based synthetic genetic interaction (SGI) analysis. We screened for modulators of cell cycle regulation by genome-wide RNAi and high-throughput imaging of *Drosophila* cells. Then we used double RNAi to systematically map the functional relationships between these genes. This analysis grouped genes into functional modules and generated hypotheses for the function of genes not previously implicated in cell cycle regulation, including *CG11753* (*Drosophila SYS1*) and *l(2)NC136* (*Drosophila CNOT3*). The results of this study demonstrate the use of synthetic genetic interaction experiments in metazoan cells to refine functional predictions from large-scale perturbation experiments.

RESULTS AND DISCUSSION

A two-step RNAi screening approach for regulators of the cell cycle

To identify and map potentially novel regulators of the cell cycle, we used high-throughput imaging to measure the effects of single and double perturbations on cell cycle–relevant phenotypes in *Drosophila* S2 cells (Figure 1A and *Materials and Methods*). First, using a genome-wide RNAi library targeting ~98% of the protein coding transcripts (Horn *et al.*, 2010; Horn and Boutros, 2013), we systematically interrogated the *Drosophila* genome for effects of single-gene knockdowns on the cell cycle. Fluorescence microscopy images of nuclei (DNA) and phospho-Histone H3–positive (pH3; phosphorylated from mitotic prophase to anaphase) cells were captured for each condition after 5 d of knockdown. We focused our analysis on three phenotypes extracted from the images: number of nuclei (cell number) as a measure of cell viability and average nuclear area and mitotic index (proportion of pH3-positive cells) as measurements directly related to cell cycle–relevant processes (*Materials and Methods*). After selecting a set of ~300 putative novel cell cycle regulators from the genome-wide data set, in a second experiment we tested double knockdowns of the candidates with 14 well-characterized cell cycle regulators using the same microscopic readouts and assessed genetic interactions. In that way, we aimed at mapping the putative novel regulators to known cell cycle processes.

Results of the genome-wide screen

To identify RNAi reagents that had effects on the cells in the genome-wide screen, we computed *z*-scores for each of the three phenotypes. For nuclear area and mitotic index phenotypes, we adjusted for cell count effects using regression analysis (*Materials and Methods*). The *z*-scores of two replicates showed strong positive correlations for all three phenotypes (Supplemental Figure S1A). By comparing *z*-scores between the three phenotypes across the entire screen, we found that they provided complementary information about the effects of gene knockdowns as indicated by their low Pearson correlation (Supplemental Figure S1B). Figure 1B highlights the information gain by assessing nuclear area and mitotic index in addition to cell count: although genes implicated in different biological processes affected cell counts similarly (or had no effect at all), they showed differential effects in the other phenotypes. For example, knocking down genes encoding sperm-specific dynein intermediate chains (*Sdic1*, *Sdic2*, *Sdic3*, *Sdic4*) or genes involved in mRNA cleavage and polyadenylation (*Cpsf100*, *Cpsf160*, and *Cpsf73*) showed mild to no effects on cell counts, but the mitotic index was increased after perturbation of the dynein intermediate chains and decreased after perturbation of the mRNA-processing factors (Figure 1C). This was also in agreement with their known implications for the cell cycle, where dyneins are required for mitotic progression and mRNA-processing factors are important during interphase (Manley, 1995; Nurminsky *et al.*, 1998). In another example, we found that genes with a role in cytokinesis could have diverging effects on the mitotic index (increased for *tum*, *pbl*, *zip*, and *scra*; decreased for *Incenp*, *borr, Det*, and *ial*), while invariably decreasing cell counts and increasing nuclear area (Figure 1C). This confirmed the requirement of the components of the chromosomal passenger complex inner centromere protein (Incenp), borealin (Borr; *Drosophila* CDCA8), and deterin (Det, *Drosophila* survivin) for Histone H3 phosphorylation by ial (aurora B kinase [aurB]; Carmena *et al.*, 2012), in contrast to the proteins tumbleweed (tum, *Drosophila* RACGAP1) and pebble (pbl, *Drosophila* ARHGEF5), which are essential for cytokinesis but do not alter phospho–Histone H3 phosphorylation (Zavortink *et al.*, 2005). Overall, assessing the three complementary phenotypes provided a more detailed view of gene functions and highlighted genes with potential roles in the cell cycle.

To get a more comprehensive picture of factors affecting nuclear area and mitotic index as markers of cell cycle progression, we filtered the results of the genome-wide screen for all treatments with an absolute *z*-score ≥3 for either of the phenotypes. Of ~15,000 genes assessed by RNAi (Supplemental Table S1), knockdowns of ~1000 (6.7%) resulted in such a phenotype (Supplemental Table S2). Approximately 17% of them were specific to nuclear area and 75% to mitotic index, and 8% scored in both phenotypes. We grouped the phenotypic profiles of the 1000 genes by hierarchical clustering of their *z*-scores (Figure 2A). This identified several clusters that were enriched for known cell cycle regulators (Figure 2, B–E). For example cluster I (Figure 2B) grouped proteins required for formation of the mitotic spindle (Teixido-Travesa *et al.*, 2012), including tubulins, as well as components of the augmin and CCT chaperonin complexes (Supplemental Table S3). Loss of function of these proteins commonly increased the mitotic index, indicating a mitotic arrest. In contrast ,cluster IV (Figure 2E) grouped components of the COP9 signalosome (CSN; Supplemental Table S3) complex, which is required during the G1/S transition of the cell cycle (Doronkin *et al.*, 2003). Knocking down CSN members commonly decreased the mitotic index, indicating a cell cycle arrest before mitosis. To address more systematically the question of which processes could be detected by our assay, we manually annotated a high-confidence list of 131 proteins with well-characterized roles during G1/S transition, the G2/M checkpoint, and the mitotic spindle, as well as regulators of mitotic progression and cytokinesis (Supplemental Table S3). We found that 96 of the known factors (73%), covering all manually annotated cell cycle processes, had an absolute *z*-score ≥3 in nuclear area and/or mitotic index (Supplemental Figure S2A), which validated our screening approach. Of interest, when comparing the phenotypes (nuclear area and mitotic index) across the different processes, we found that they affected the phenotypes differently (Supplemental Figure S2, B–D), which confirmed the previous observation that the measurement of different phenotypes was required to be able to assay different cell cycle processes.

The genome-wide screen identified many components with phenotypes similar to those of known cell cycle regulators

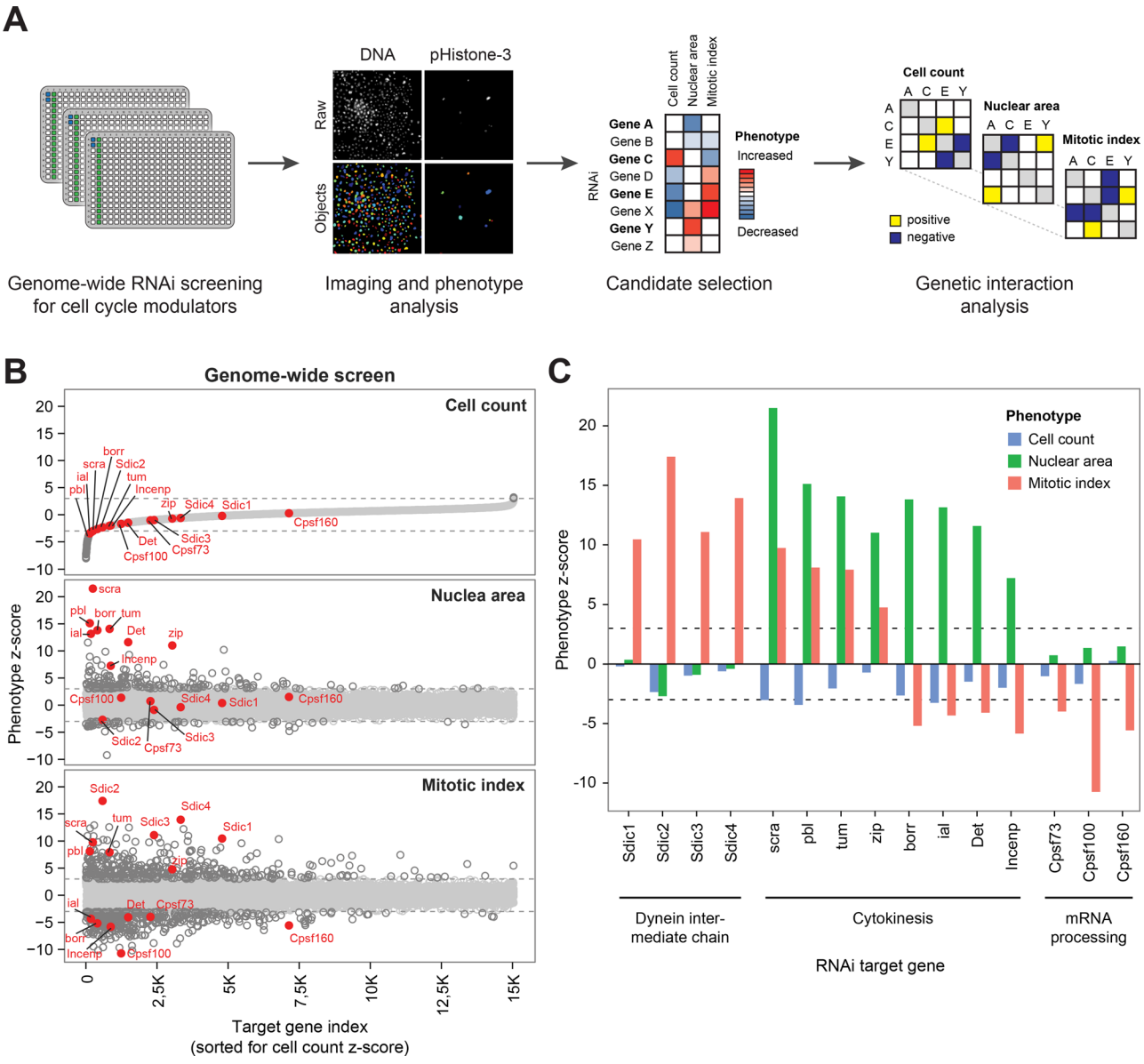

FIGURE 1: Setup of the combined genome-wide RNAi and synthetic genetic interaction analysis using multiple phenotypic readouts. (A) Genome-wide RNAi screening and high-throughput imaging to quantify the number of cells, nuclear area, and mitotic index are used to identify cell cycle regulators, which are further characterized by genetic interaction analysis. See the text for details. (B) Comparison of the three phenotypes across the genome-wide data set. The knockdown conditions (*x*-axis) are sorted according to their cell count phenotype (top). Nuclear area (middle) and mitotic index (bottom) phenotypes are shown in the same order. Highlighted in red are proteins that show differential effects across the phenotypes. Dashed lines indicate *z*-score cut-offs of 3 and −3 (points below the cut-offs are light gray, and points above are dark gray). (C) Bar plots comparing the phenotypes (per functional group) for the knockdowns highlighted in B. Knockdowns of dynein IC proteins and mRNA-processing factors show opposing effects on mitotic index and have no effects on the other phenotypes. Knockdowns of proteins required for cytokinesis all increase the nuclear area, whereas they have opposing effects on mitotic index. Dashed lines indicate *z*-score cut-offs of 3 and −3.

(Figure 2, A–E). We attempted to use genetic interaction analysis to elucidate their functional relationship with the known cell cycle machinery. To this end, we selected genes from the genome-wide screen that were expressed and displayed mitotic index and nuclear area phenotypes, prioritizing genes that had not been linked to cell cycle regulation previously (Bettencourt-Dias *et al.*, 2004; Bjorklund *et al.*, 2006; Kondo and Perrimon, 2011). We also excluded genes that were not conserved in humans, as well as genes with strong viability defects (for details of candidate selection, see the Supplemental Methods). This left us with 275 potential novel modulators from the genome-wide screen to be subjected to genetic interaction analysis: 238 with mitotic index phenotypes and 37 with nuclear area phenotypes (Supplemental Table S4). In addition we included several controls: genes with known roles in cell cycle regulation that also scored in the genome-wide screen, such as components of the anaphase-promoting

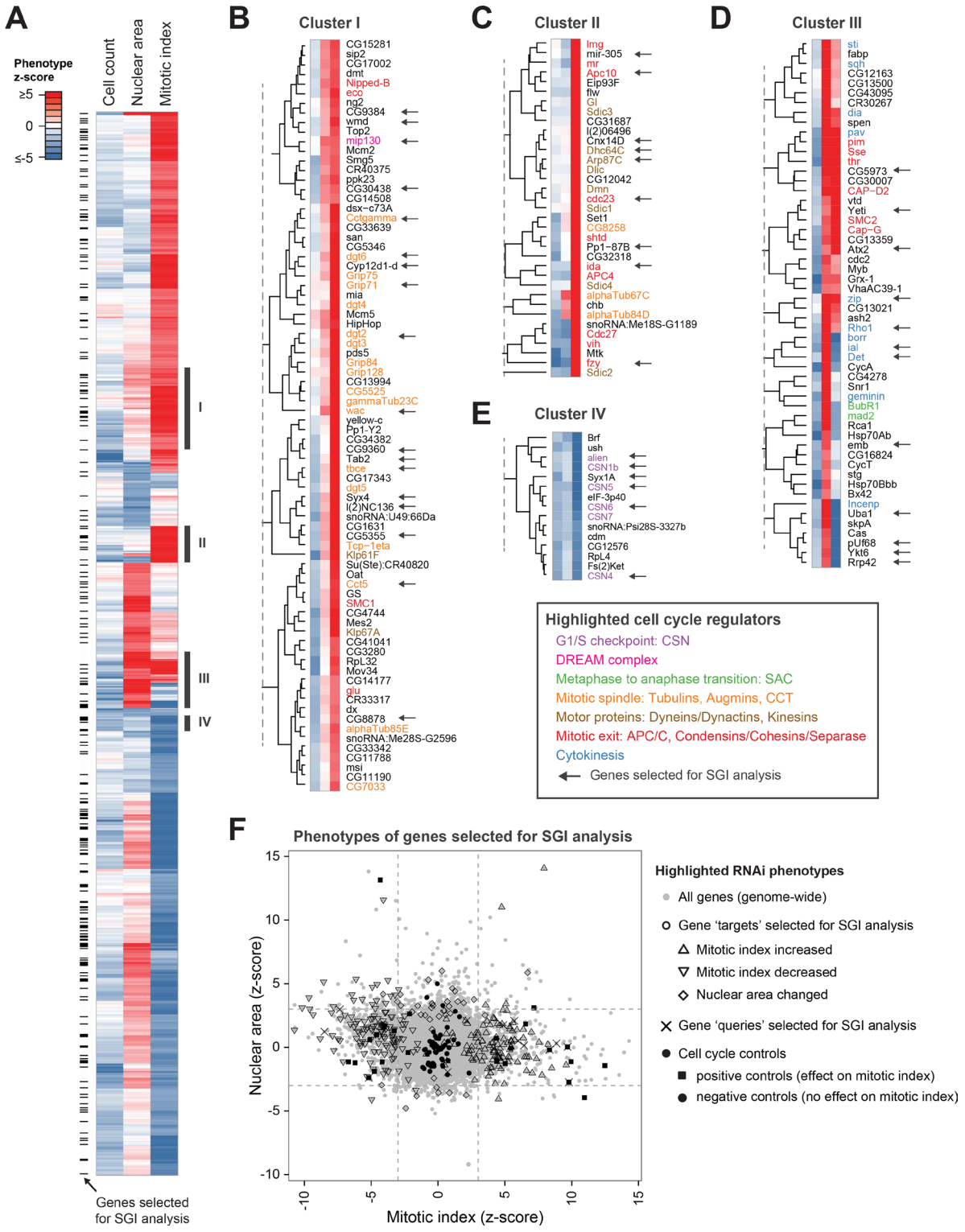

FIGURE 2: Genome-wide RNAi screening identifies known and potential novel regulators of cell cycle. (A) Heatmap of *z*-scores for 1018 genes with an absolute *z*-score ≥ 3 in nuclear area and/or mitotic index after hierarchical clustering. Black bars to the left of the heatmap highlight genes that were selected for the SGI analysis. Bars on the right of the heatmap highlight clusters of genes that are enriched for factors with known roles in cell cycle and are shown in greater detail in B–E. (B–E) Detailed heatmaps of the clusters highlighted in A. Colors of gene names indicate their membership in certain groups of cell cycle regulators (see box). Arrows highlight genes that were selected for SGI analysis. See the text for details. (F) Scatter plot of nuclear area and mitotic index phenotypes for genes selected for SGI analysis (black) on top of the genome-wide data (gray). The distribution of candidates and controls selected for the SGI analysis shows that it is representative of the effect range observed in the genome-wide screen. Different types of candidates and controls are indicated by shape (see legend and Supplemental Tables S4 and S5). APC/C, anaphase-promoting complex/cyclosome; CCT, cytosolic chaperonin–containing t-complex; CSN, COP9 signalosome; SAC, spindle assembly checkpoint.

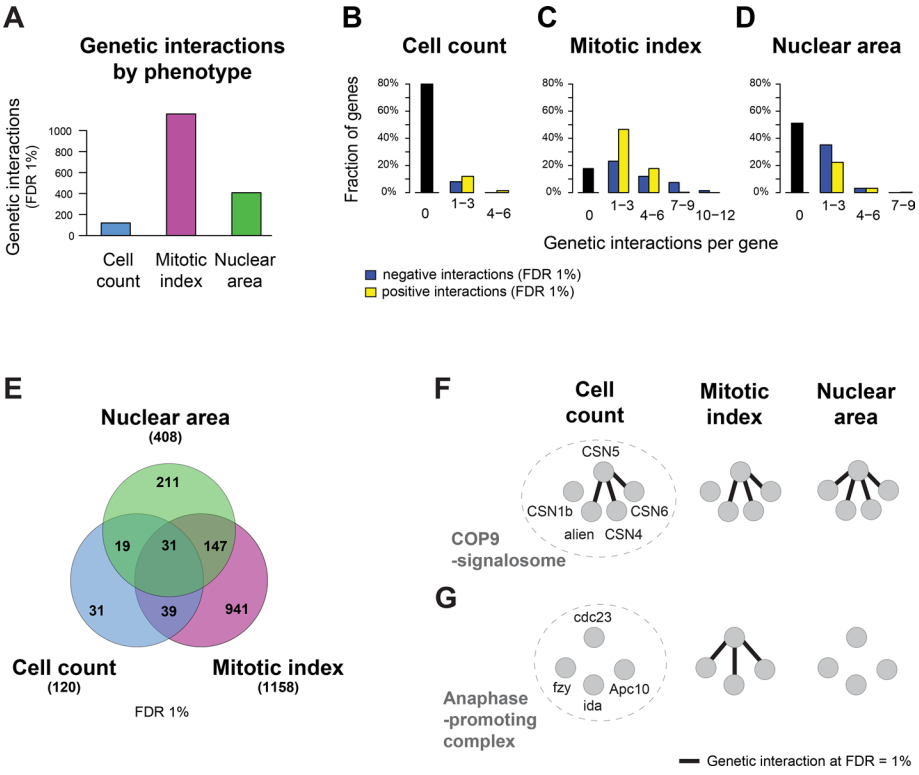

FIGURE 3: Genetic interactions across different phenotypes. (A) Comparing the number of genetic interactions affecting cell count, mitotic index, or nuclear area shows that the majority of interactions are found for the mitotic index phenotype. Interactions were estimated from a set of 14 "query" genes and 350 "candidate" genes/controls. (B–D) Node degree distributions showing number of positive (yellow bars) and negative (blue bars) genetic interactions per phenotype and on a per-gene basis. (E) A Venn diagram shows that there are overlapping, but also many exclusive, genetic interactions between the phenotypes. (F, G) Genetic interactions within the CSN largely overlap between the phenotypes (F), whereas genetic interactions within the APC/C are exclusive to the mitotic index (G). In F and G. all genetic interactions are alleviating, that is, were less severe than expected according to the reference model. All genetic interactions were called at FDR of 1%.

For cell count, mitotic index, and nuclear area phenotypes we observed 1419 genetic interactions at an experiment-wide false-discovery rate (FDR) of 1%. The mitotic index yielded a ~10- and 3-fold higher rate of genetic interactions than cell count and nuclear area, respectively (Figure 3A), which might be due to the phenotypes of the candidates that were mostly mitotic index effects (Supplemental Table S4). We assessed the node degree distribution for each phenotype (Figure 3, B–D). The majority of genes had only few interactions (Figure 3, B–D, 1–3) independent of the phenotype. The number of positive and negative interactions tended to be unbalanced, and the strongest differences were seen for the mitotic index phenotype. Here many genes had a few positive interactions (Figure 3C, 1–3), and a few genes had many negative interactions (Figure 3C, 7–9). By comparing the genetic interactions between phenotypes, we found that only 31 gene pairs interacted in all three phenotypes. In contrast, 1183 gene pairs (83.4%) displayed interactions specific for a single phenotype (Figure 3E). Whereas genetic interactions between some known cell cycle regulators, such as the members of the CSN complex, were observed in all three phenotypes (Figure 3F), other regulators, including the APC/C subunits *cdc23*, *ida*, *Apc10*, and *fzy*, showed genetic interactions for the mitotic index phenotype only (Figure 3G). This indicated that measuring different cell cycle–relevant phenotypes might be required to connect novel genes to known processes.

complex/cyclosome (APC/C) and the CSN complex, as well as genes that had no or only mild effects on the phenotypes of interest, in order to prevent biases during the analysis of genetic interactions. The list of candidates covered a broad range of mitotic index and nuclear area phenotypes, representative of the range of effects observed in the genome-wide screen (Figure 2F).

Different phenotypes identify nonredundant genetic interactions

To test the set of candidates from the genome-wide screen for genetic interactions, we systematically codepleted them with 14 known cell cycle regulators ("query" genes, Supplemental Table S5) in all pairwise "candidate × query" combinations. To reduce the influence of potential off-target effects on the interaction analysis, we used two sequence-independent RNAi reagents to target each candidate and each query gene, resulting in 20,216 co-RNAi experiments with four independent measurements per gene pair. This experimental setup was shown previously to allow robust estimation of single- and double-RNAi phenotypes (Horn *et al.*, 2011). Genetic interactions and their significance were measured independently for each phenotype as deviations from the multiplicative model, which describes the expected combinatorial effect as the product of the single-knockdown effects, and are summarized in π-scores (Supplemental Table S6).

Phenotype-specific interaction networks functionally connect candidate genes

To systematically predict functional associations of candidate genes, we assessed the similarity of their genetic interaction profiles. This type of analysis was previously shown to provide robust approximations of functional associations (Costanzo *et al.*, 2010; Fuxman Bass *et al.*, 2013). We first calculated the Pearson correlation coefficient (PCC) between the interaction profiles of all candidates for each phenotype. To correct for genes that shared a high PCC with many genes, we transformed the PCC data into the connection specificity index (CSI; Figure 4A), which reduces potential nonspecific similarities between genes by ranking the similarities according to the connectivity of their interaction partners (Green *et al.*, 2011; Fuxman Bass *et al.*, 2013).

We assessed whether the CSI improved functional associations between candidate genes compared with their single-knockdown phenotypes. As expected, using the mitotic index, all APC/C components tested (*ida*, *cdc23*, and *fzy*) had a high mitotic index–based CSI with *Apc10* (Figure 4B). In contrast, components of the Augmin complex (*wac, dgt2*) and the DREAM complex (*mip120, mip130*) shared a lower CSI with *Apc10*, despite their similar single-knockdown effect on mitotic index (Figure 4B). Several other genes, such as the known modulator of mitosis *pontin* (*pont*, a member of the INO80/SWR1 chromatin-remodeling complexes; Ducat *et al.*, 2008),

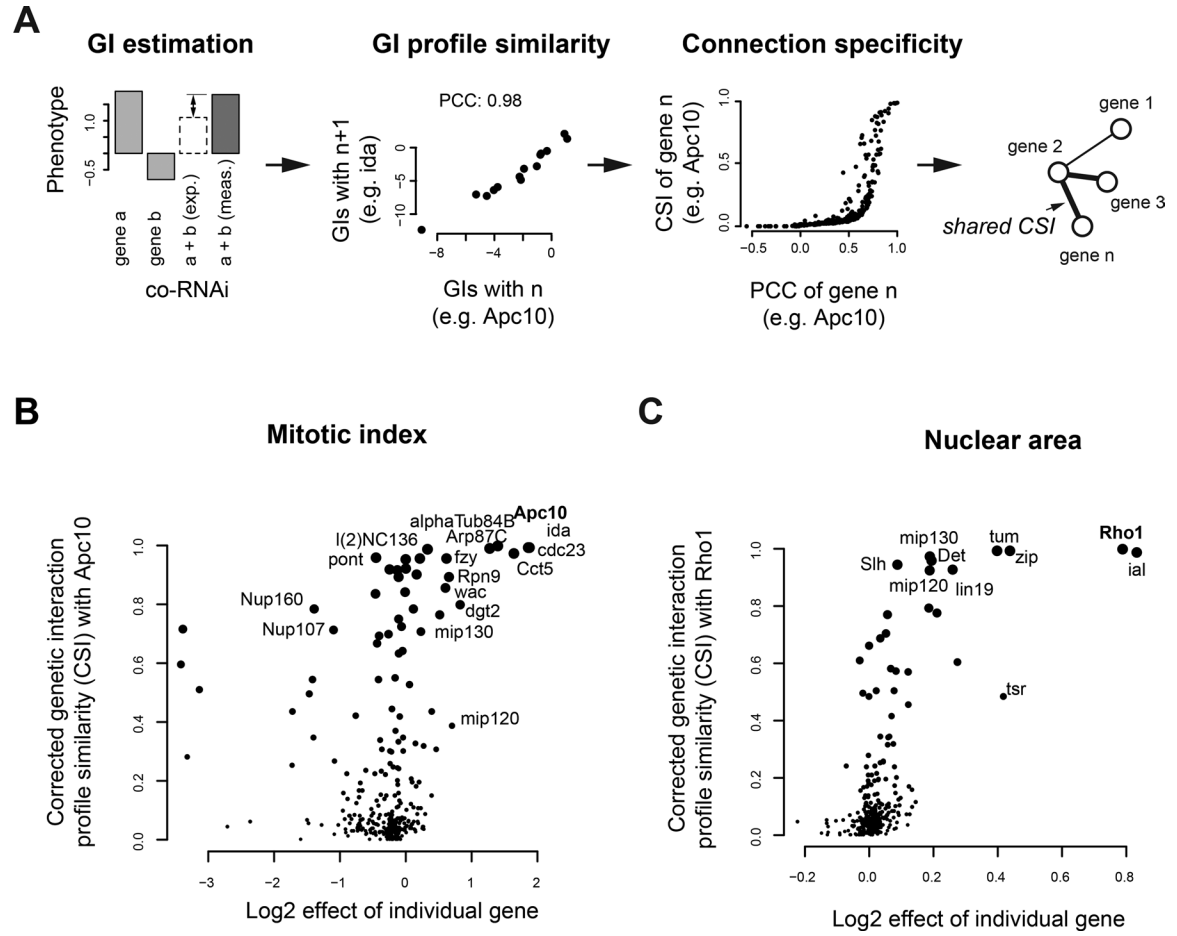

FIGURE 4: Genetic interaction profiles associate genes with similar functions. (A) Processing of genetic interaction (GI) profiles to predict functional similarity between genes. The profiles (14 π-scores) of each candidate gene pair were compared per phenotype by calculating the PCC. The example shows the PCC between the mitotic index–based profiles of the APC/C components *Apc10* and *ida*. The PCC was corrected by calculating the CSI with a correction factor/constant of 0.01. The example shows the relation between the PCC and CSI of Apc10. (B) Comparison of the mitotic index–based CSI connecting *Apc10* to all tested genes with the single-knockdown effect of all genes shows additional APC/C components (and cell cycle regulators) in proximity to *Apc10*. (C) Comparison of the nuclear area–based CSI connecting *Rho1* to all tested genes with the single-knockdown effect of all genes shows additional cytokinesis components (and cell cycle factors) in proximity to *Rho1*. See the text for details. The point size is proportional to the CSI in B and C.

also had a high CSI with *Apc10* without increasing the mitotic index when depleted alone (Figure 4B), drawing a potential connection to the APC/C. We also compared the nuclear area–based CSI of the cytokinesis regulator *Rho1* to the single-knockdown effects of all other genes. This highlighted many known cytokinesis factors (e.g., *tum*, *zip*, *Det*) but deprioritized other, likely functionally independent genes that also showed an increased nuclear area, such as *twinstar* (*tsr*, *Drosophila* cofilin), a component required for mitotic telophase and cytokinesis (Gunsalus *et al.*, 1995; Figure 4C). These results show that the CSI could highlight genes with similar functions that could not be differentiated based on their single-knockdown effects.

To identify association more systematically for each phenotype, we placed all candidate genes in a force-directed network according to their functional similarity (CSI; Figure 5, A and B, and Supplemental Figure S5A). The mitotic index–based network associated the APC/C with components facilitating mitotic spindle organization and regulation, including dynactin subunits (Arp87C) and the CCT chaperonin complex member Cct5 (Figure 5A). These close associations with the APC/C were not seen for the other phenotypes (Figure 5B and Supplemental Figure S5, A and B). In the proximity of APC/C, we observed additional interesting connections. We already highlighted the high CSI of the INO80/SWR1 complex member pont with Apc10. We found more members of different chromatin-remodeling complexes in the proximity of the APC/C, including domino (dom) and Yeti (both members of SWR1), Nurf-38 (a member of the NURF complex), and female sterile homeotic (fs(1)h, a BET-family protein). Further, several genes involved in regulation of transcription, such as *pointed* (*pnt*, ETS transcription factor) and *l(2)NC136* (*Not3*, a member of the CCR4-NOT deadenylation complex), were connected to the APC/C. These results suggested a specific role for regulation of chromatin and transcription during mitosis (Morrison and Shen, 2009; Tanenbaum *et al.*, 2015). Other processes/complexes in the proximity of the APC/C included the DREAM complex (mip120, mip130), which was previously shown to regulate mitotic events

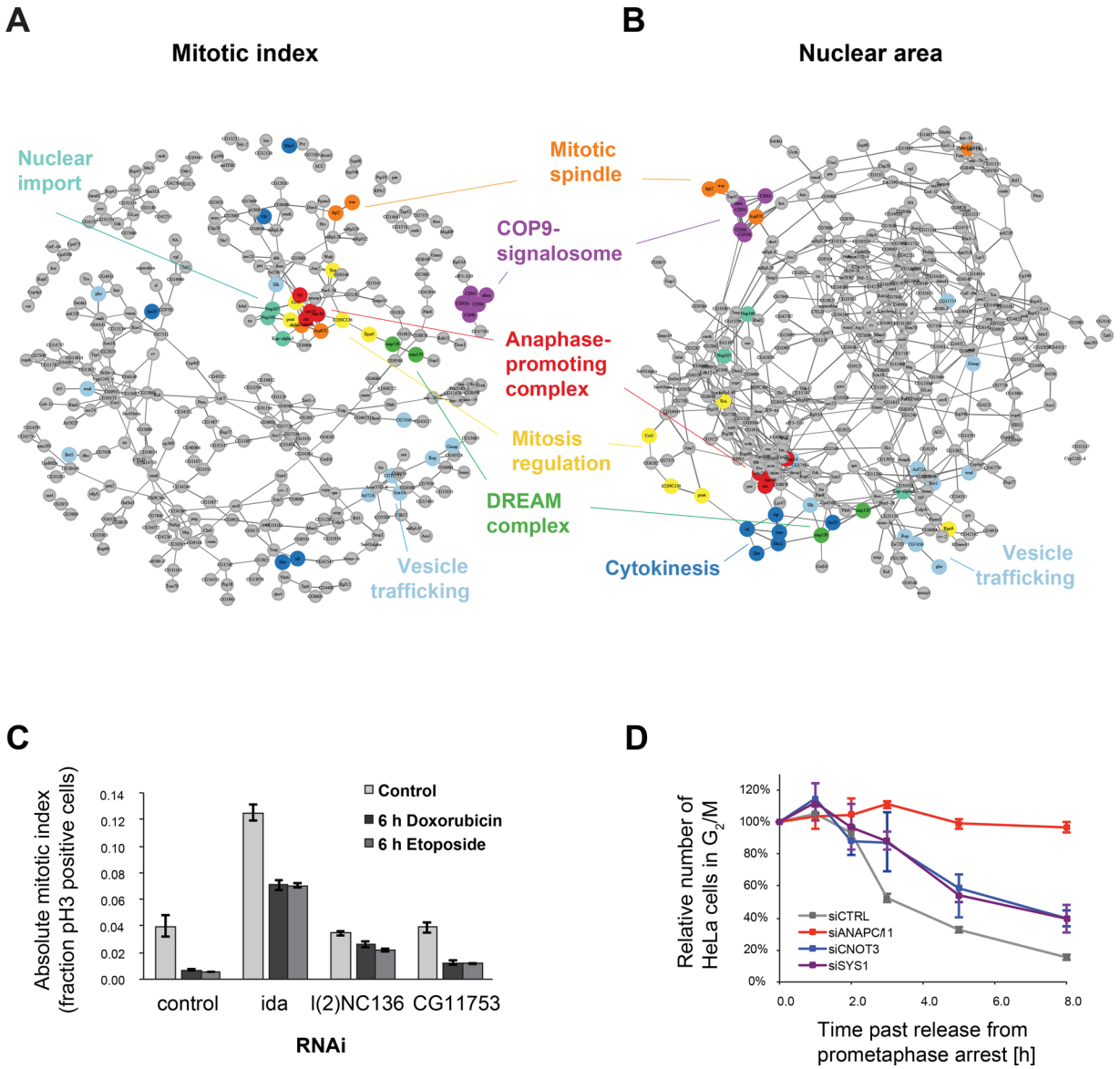

FIGURE 5: Networks based on cell cycle–relevant phenotypes. (A) Mitotic index–based and (B) nuclear area–based functional associations of candidate genes show known cell cycle processes (different colors) linked to each other and to uncharacterized genes/processes. Genes were placed in a force-directed network based on the genetic interactions for each phenotype. Only gene pairs (connections) with CSI > 0.95 are shown. (C) *l(2)NC136* and *CG11753* are required for mitotic progression in *Drosophila* cells. Each gene was knocked down by two independent dsRNA designs, *ida* was knocked down as positive control, and firefly luciferase was used as negative control. At 96 h past dsRNA transfection, the G2/M checkpoint was triggered by doxorubicin or etoposide, and cells were allowed to leave M phase for 6 h before assessment of the mitotic index. The data show the mean of 32 (control) or 4 (*ida*, *l(2)NC136*, *CG11753*) replicates, and the error bars indicate SEM. (D) Functional depletion of the human orthologues of *l(2)NC136* and *CG11753* (*CNOT3* and *SYS1*, respectively) using siRNAs for 72 h shows a delayed mitotic exit after release from prometaphase arrest in HeLa cells. Prometaphase arrest was induced by nocodazole treatment for 18 h, and the fraction of G2/M cells was assessed at different time points after release by fluorescence-activated cell sorting analysis. The data show the mean of three replicates; the error bars indicate SEM.

(Beall *et al.*, 2004; Georlette *et al.*, 2007), and the regulators of nuclear import *Nup107*, *Nup160*, and *Kap-alpha3*. The latter finding suggested a role for nuclear pore complex components during mitosis that has been described before (Loiodice *et al.*, 2004). Other subnetworks highlighted known cell cycle–regulatory complexes, such as the CSN, but also processes that are less well understood in the context of the cell cycle, such as vesicle trafficking.

The mitotic index–based network failed to identify known functional associations between cytokinesis regulators (Figure 5A and Supplemental Figure S5C). In contrast, the nuclear area–based network connected Rho1 with other components of cytokinesis (tum, ial, Det, lin19, and zip; Figure 5B). Of interest, several regulators of vesicle trafficking and exocytosis were found in subnetworks connected to cytokinesis, suggesting a potential role of exocytosis during cytokinesis that has been previously described

(Skop *et al.*, 2001). Although vesicle components grouped in the mitotic index–based network as well (e.g., *Arf72A*, *CG11753*, *Syx1A*), they were not connected directly to any of the other known processes, which highlights the information gain from generating phenotype-specific networks. Despite the conservation of some subnetworks across all three phenotypes, such as the CSN or the APC/C, the connections between the processes and uncharacterized genes were phenotype specific. With mitotic index–based and nuclear area–based networks being stronger indicators of cell cycle–specific processes (Figure 5, B and C), this provided us with testable hypotheses for potentially novel regulators of the cell cycle.

Golgi-resident and mRNA processing factors modulate mitotic progression

To assess the validity of our network-based prediction of gene functions, we tested the role of two genes in cell cycle–relevant assays. The mitotic index–based network connected the APC/C and other regulators of mitosis to chromatin-remodeling complexes and transcriptional regulators. We followed up on one of the genes in proximity to the APC/C, *l(2)NC136*, which is a member of the conserved deadenylation complex CCR4-NOT. Its human orthologue, *CNOT3*, regulates mitotic progression by destabilizing the mRNA of the spindle assembly checkpoint (SAC) component *MAD1* (Takahashi *et al.*, 2012). To confirm the predicted role for *l(2)NC136*, we knocked down the gene in *Drosophila* S2 cells with double-stranded RNAs (dsRNAs) for 4 d and triggered a G_2/M checkpoint arrest by doxorubicin or etoposide treatment for 6 h to allow cells with intact mitotic progression machinery to exit M phase (Figure 5C). Cells depleted of *l(2)NC136* displayed approximately fourfold higher frequency of pH3-positive nuclei in both treatments than with a control knockdown, indicating a delay in mitotic exit. To validate the conserved function of *l(2)NC136* in human cells, we knocked down its orthologue, *CNOT3*, in HeLa cells using siRNAs and assessed the cycle after release from a nocodazole-induced prometaphase arrest. Similarly to *Drosophila* cells, HeLa cells displayed a significant mitotic delay (assessed by quantifying G_2/M-phase contents; $p < 0.019$, paired Student's *t* test) after knockdown of CNOT3 (Figure 5D and Supplemental Figure S5D) compared with a control siRNA. These results confirmed a role of *l(2)NC136* during mitotic exit, as suggested by the network-based predictions.

Another process highlighted in both the mitotic index–based and nuclear area–based networks is vesicular trafficking. Several components of this network were previously shown to have cell cycle–specific functions. For example, *syntaxin1A* (*syx1A*), which encodes for a target–soluble *N*-ethylmaleimide–sensitive factor attachment protein receptor, was shown to be required for mitotic telophase (Somma *et al.*, 2002). *Gmap* and *Arf72A* are crucial for Golgi inheritance during cell division (Rios *et al.*, 2004; Eisman *et al.*, 2006). These genes formed a subgroup in the mitotic index–based network also containing the largely uncharacterized gene *CG11753* (Figure 5B). Its human orthologue, *SYS1*, has been shown to have a function during Golgi-targeted vesicular transport (Behnia *et al.*, 2004; Setty *et al.*, 2004). In agreement with its predicted role, depletion of CG11753 in *Drosophila* S2 cells and SYS1 in HeLa cells delayed mitotic progression (Figure 5, C and D).

The mitosis phenotypes seen for *l(2)NC136*/*CNOT3* and *CG11753*/*SYS1* in independent assays in *Drosophila* and human cells showed that hypothesis generated from mitotic index– or nuclear area–based interaction networks could be validated. Future studies could address in a more detailed way the manner in which regulation of transcription and vesicular traffic connect to cell cycle/mitosis. Further, additional subnetworks could be subjected to similar follow-up analysis to understand their role during the cell cycle.

Conclusion

This study demonstrates how unbiased, genome-wide screening followed by genetic interaction analysis can fine-tune predictions of gene function and guide follow-up experimentation by providing more specific and testable hypotheses. Of importance, predictions of gene functions from interactions based on phenotypes relevant to the biology examined, such as mitotic index and nuclear area to assay cell cycle, were superior to predictions of gene functions from viability/cell count–based interactions. Genetic interaction networks based on relevant phenotypes reconstructed known functional relations during mitotic progression and cytokinesis and suggested potentially novel regulators. We validated novel roles for an mRNA-processing component and a Golgi-vesicular transport protein during mitotic exit.

With automated imaging being a versatile tool to simultaneously record multiple quantitative phenotypes (Perlman *et al.*, 2005; Fuchs *et al.*, 2010; Fischer *et al.*, 2015), this approach could be expanded to other biological processes by assaying relevant markers. Established reporter-based readouts to monitor the activity of signaling pathways could also be used to perform genetic interaction analysis, and differential networks could be built from experiments using different ways to activate or suppress the pathway.

MATERIALS AND METHODS

Drosophila tissue culture

We cultured Schneider S2 cells adjusted to serum-free growth medium (D.Mel-2; ThermoFisher, Waltham, MA) in Express Five SFM supplemented with 20 mM GlutaMAX and 1% penicillin-streptomycin (all from Invitrogen by ThermoFisher).

RNAi library

We used a genome-wide RNAi library targeting ~98% of all coding genes in the *Drosophila* genome designed against FlyBase annotations for the *Drosophila melanogaster* Berkeley *Drosophila* Genome Project genome, releases 4 and 5, using NEXT-RNAi software (Horn *et al.*, 2010). In addition, the library covered 1254 strongly expressed regions from the Heidelberg predictions (Heidelberg Collection) of *Drosophila* genes not covered by FlyBase (Hild *et al.*, 2003). Primer and dsRNA sequence information, target mappings, and the analysis of specificity and additional features of the dsRNA designs are available through GenomeRNAi (www.genomernai.org; Schmidt *et al.*, 2013). For screening, the library was aliquoted in 384-well plates (black/clear; BD Falcon) with an average of 250 ng of dsRNA/well in 5 µl of water.

Genome-wide RNAi screening

In each biological replicate, we seeded 6500 cells in 40 µl of culture medium with 0.2 µl of 0.4 mg/ml dimethyldioctadecylammonium bromide (DDAB) per well (in black/clear 384-well plates; BD Falcon) and incubated the plates for 5 d at 25°C before fixation, staining, and imaging of cells.

Cell staining and imaging

Cell stainings were done using a Beckman Biomek FX robot with 384-well tip head. First, of the 40 µl of assay volume, 15 µl was removed, and cells were fixed/permeabilized for 60 min at room temperature by addition of 40 µl of a 6% paraformaldehyde (Sigma-Aldrich, St. Louis, MO)/0.3% Triton X-100 (AppliChem, Darmstadt, Germany) solution in phosphate-buffered saline (PBS; Sigma-Aldrich).

Cells were washed by removing 40 µl of supernatant and adding of 50 µl of PBS. Next 50 µl of the supernatant was removed, and 10 µl of a monoclonal phospho–Histone H3 antibody (conjugated to Alexa Fluor 647; 3458; Cell Signaling) diluted 1:750 in 4% bovine serum albumin (GERBU, Heidelberg, Germany)/0.1% Triton X-100 (in PBS) was added and incubated overnight at 8°C (protected from light). On the next day, 10 µl of supernatant was removed, and DNA was stained by addition of 40 µl of Hoechst 33342 (Invitrogen) diluted 1:2000 in PBS with incubation for 30 min at room temperature. Finally, cells were washed once by removing 40 µl of supernatant and adding 50 µl of PBS and washed two more times by removing 50 µl of supernatant and adding 50 µl of PBS. Plates were sealed with aluminum sealing tape (Corning, Corning, NY) and imaged directly or stored at 8°C until imaging. Fluorescence images were acquired on an IN Cell Analyzer 2000 (GE Healthcare, Little Chalfont, UK) using a 4× objective, which enables capture of the entire well in one image. One image was acquired for each of the two channels (Hoechst and phospho–Histone H3 antibody).

Image analysis

Image analysis and feature extraction from the 4× images (16 bit, 2048 × 2048 pixels) were performed using the R/Bioconductor package EBImage (Pau *et al.*, 2010). The nuclei were segmented and identified separately for the Hoechst and phospho-H3 channels. Adaptive thresholding (width of moving window, 4 pixels) was used to separate nuclei areas from the image background. Nuclei were identified by local-maximum search on the fluorescence images. The nuclei areas were extended from the local maxima by a propagation algorithm (Jones *et al.*, 2005). Nearest-neighbor search was used to match phospho-H3 objects to nuclei in the Hoechst channel (only mitotic nuclei were visible in the phospho-H3 channel). Matches were accepted if the distance between the centers of the objects in both channels was <5 pixels. Eighty-four quantitative features were extracted, of which we focused on three: nuclei count (a correlate of cell count), mitotic index (the ratio of nuclei in the phospho-H3 channel and the Hoechst channel), and nuclear area.

Computational analysis of the genome-wide RNAi screen

Raw data of each feature were first $\log_2$-transformed. To account for row and/or column effects, a local polynomial regression (loess) on the spatial coordinates was fitted to each plate and subtracted. Loess-normalized values were further adjusted for the plate variance, generating *z*-scores. Replicates were summarized for each feature by taking the median. We focused on three of the features: the number of cells per well, the mitotic index, and the average nuclear area. Overall a nonlinear trend was observed between cell count and the other two phenotypes (nuclear area, mitotic index). We calculated a model (using loess regression) to adjust for cell count effect on these phenotypes and computed *z*-scores from the residuals (Supplemental Table S1). The heatmap of *z*-scores in Figure 2A was generated using hierarchical clustering based on Euclidean distances.

Combinatorial RNAi

For the double-RNAi screen, we used a candidate-sensitizer design. We pipetted 125 ng (2.5 µl) of each candidate dsRNA into a 384-well clear-bottom microscopy plate (BD Falcon) as described. Then we added 125 ng (2.5 µl) of one of the sensitizer dsRNAs using a NanoDrop II dispenser (Innovadyne), creating ~21,000 combinations (28 sensitizer vs. 750 candidate dsRNAs). Each pairwise combination of genes was assayed through four pairs of independent dsRNA designs: if we denote by A and A′ the two independent designs targeting one gene and by B and B′ the two independent dsRNA reagents targeting the other, then each biological replicate of the experiment contained the candidate–sensitizer combinations A-B, A-B′, A′-B, and A′-B′. In each well, 6500 cells were seeded in 30 µl of culture medium with 0.15 µl of 0.4 mg/ml DDAB per well and incubated for 5 d at 25°C before fixation, staining, and imaging of cells (using the methods described for the genome-wide screen).

Mathematical modeling of synthetic genetic interactions

As described previously (Axelsson *et al.*, 2011; Horn *et al.*, 2011), we used a multiplicative model as the reference model (null model), which assumes that the double-RNAi phenotypic effect of noninteracting genes is equal to the product of the single-RNAi phenotypic effects. The single-RNAi phenotypic effects (main effects) for the 14 "query" genes were estimated by taking the median effect over all candidate genes (per phenotype). To prevent biases for the main-effect estimates of candidate genes, their main effects were estimated using measurements after the gene was codepleted with control dsRNAs (targeting nonexpressed firefly luciferase). Pairwise interaction scores were then computed as the log ratio of the measured phenotype and the predicted phenotype (from the reference model), which is the product of the two single-knockdown effects. The significance of an interaction was assessed by calculating the deviation from zero from four interaction scores per gene pair (four independent co-RNAi experiments per gene pair). To this end, a moderated *t* test (R/Bioconductor package limma) was used, which first estimates the standard errors (SEM) by fitting a linear model through the four values, followed by empirical Bayes smoothing of the SEM (Smyth, 2004). The *p* values were adjusted for multiple testing by the method of Benjamini and Hochberg (1995) controlling the FDR.

Calculation of the connection specificity index on the similarity between genetic interaction profiles

The CSI is based on a correlation matrix. For each pair of target genes, the PCC of the two genetic interaction profiles along all query genes was computed. The CSI of a gene pair A-B was then defined as the fraction of genes connected to A and B that have a PCC smaller than the PCC of A and B. A constant of 0.01 was applied in the CSI definition of Green *et al.* (2011).

Induction of G_2/M checkpoint arrest in *Drosophila* S2 cells

To test the mitotic arrest after RNAi against genes selected from the primary screen, we triggered G_2/M checkpoint arrest in *Drosophila* S2 cells 96 h past dsRNA transfection using 4 µM doxorubicin or 20 µM etoposide. After 6 h, cells were fixed and stained for their DNA content (Hoechst 33342) and for pH3, and their mitotic index phenotype was determined (for details see the Supplemental Methods).

Fluorescence-activated cell sorting–based analysis of mitotic exit in human HeLa cells

Human HeLa cells were transfected with siRNA pools targeting the gene of interest and cultured for 3 d under standard conditions. A prometaphase arrest was induced by applying 40 ng/ml nocodazole for 18 h under standard conditions, and cells were released from this arrest and fixed at different time points up to 8 h postrelease. After propidium iodide staining, cell cycle profiles were determined using fluorescence-activated cell sorting analysis, counting 10,000 events/sample (for details, see the Supplemental Methods).

Data access

Supplemental Tables S1–S7, Figures S1–S5, and Supplemental Material and Methods provide all interaction (π) scores and *p* values.

ACKNOWLEDGMENTS

We thank the members of the Boutros and Huber labs for helpful discussions and Y. Kimata for comments on the manuscript. T.S. was supported by a CellNetworks postdoctoral fellowship and T.H. by a fellowship from the Studienstiftung. M.Bi. is supported by a Ph.D. fellowship from the Helmholtz International Graduate School for Cancer Research. Research in the laboratory of M.B. is supported by grants from the European Research Council and the Helmholtz Society. W.H. and B.F. acknowledge funding from the European Commission NoE Systems Microscopy.

REFERENCES

Axelsson E, Sandmann T, Horn T, Boutros M, Huber W, Fischer B (2011). Extracting quantitative genetic interaction phenotypes from matrix combinatorial RNAi. BMC Bioinformatics 12, 342.

Bakal C, Linding R, Llense F, Heffern E, Martin-Blanco E, Pawson T, Perrimon N (2008). Phosphorylation networks regulating JNK activity in diverse genetic backgrounds. Science 322, 453–456.

Beall EL, Bell M, Georlette D, Botchan MR (2004). Dm-myb mutant lethality in Drosophila is dependent upon mip130: positive and negative regulation of DNA replication. Genes Dev 18, 1667–1680.

Behnia R, Panic B, Whyte JR, Munro S (2004). Targeting of the Arf-like GTPase Arl3p to the Golgi requires N-terminal acetylation and the membrane protein Sys1p. Nat Cell Biol 6, 405–413.

Benjamini Y, Hochberg Y (1995). Controlling the false discovery rate: a practical and powerful approach to multiple testing. J R Stat Soc B Stat Methodol 57, 289–300.

Bettencourt-Dias M, Giet R, Sinka R, Mazumdar A, Lock WG, Balloux F, Zafiropoulos PJ, Yamaguchi S, Winter S, Carthew RW, *et al.* (2004). Genome-wide survey of protein kinases required for cell cycle progression. Nature 432, 980–987.

Bjorklund M, Taipale M, Varjosalo M, Saharinen J, Lahdenpera J, Taipale J (2006). Identification of pathways regulating cell size and cell-cycle progression by RNAi. Nature 439, 1009–1013.

Boutros M, Ahringer J (2008). The art and design of genetic screens: RNA interference. Nat Rev Genet 9, 554–566.

Boutros M, Kiger AA, Armknecht S, Kerr K, Hild M, Koch B, Haas SA, Paro R, Perrimon N (2004). Genome-wide RNAi analysis of growth and viability in Drosophila cells. Science 303, 832–835.

Carmena M, Wheelock M, Funabiki H, Earnshaw WC (2012). The chromosomal passenger complex (CPC): from easy rider to the godfather of mitosis. Nat Rev Mol Cell Biol 13, 789–803.

Carpenter AE, Sabatini DM (2004). Systematic genome-wide screens of gene function. Nat Rev Genet 5, 11–22.

Collins SR, Miller KM, Maas NL, Roguev A, Fillingham J, Chu CS, Schuldiner M, Gebbia M, Recht J, Shales M, *et al.* (2007). Functional dissection of protein complexes involved in yeast chromosome biology using a genetic interaction map. Nature 446, 806–810.

Costanzo M, Baryshnikova A, Bellay J, Kim Y, Spear ED, Sevier CS, Ding H, Koh JL, Toufighi K, Mostafavi S, *et al.* (2010). The genetic landscape of a cell. Science 327, 425–431.

DasGupta R, Kaykas A, Moon RT, Perrimon N (2005). Functional genomic analysis of the Wnt-wingless signaling pathway. Science 308, 826–833.

Dixon SJ, Fedyshyn Y, Koh JL, Prasad TS, Chahwan C, Chua G, Toufighi K, Baryshnikova A, Hayles J, Hoe KL, *et al.* (2008). Significant conservation of synthetic lethal genetic interaction networks between distantly related eukaryotes. Proc Natl Acad Sci USA 105, 16653–16658.

Doronkin S, Djagaeva I, Beckendorf SK (2003). The COP9 signalosome promotes degradation of Cyclin E during early Drosophila oogenesis. Dev Cell 4, 699–710.

Ducat D, Kawaguchi S, Liu H, Yates JR 3rd, Zheng Y (2008). Regulation of microtubule assembly and organization in mitosis by the AAA+ ATPase Pontin. Mol Biol Cell 19, 3097–3110.

Eisman RC, Stewart N, Miller D, Kaufman TC (2006). Centrosomin's beautiful sister (cbs) encodes a GRIP-domain protein that marks Golgi inheritance and functions in the centrosome cycle in Drosophila. J Cell Sci 119, 3399–3412.

Fischer B, Sandmann T, Horn T, Billmann M, Chaudhary V, Huber W, Boutros M (2015). A map of directional genetic interactions in a metazoan cell. Elife 4, doi: 10.7554/eLife.05464.

Fuchs F, Pau G, Kranz D, Sklyar O, Budjan C, Steinbrink S, Horn T, Pedal A, Huber W, Boutros M (2010). Clustering phenotype populations by genome-wide RNAi and multiparametric imaging. Mol Syst Biol 6, 370.

Fuxman Bass JI, Diallo A, Nelson J, Soto JM, Myers CL, Walhout AJ (2013). Using networks to measure similarity between genes: association index selection. Nat Methods 10, 1169–1176.

Georlette D, Ahn S, MacAlpine DM, Cheung E, Lewis PW, Beall EL, Bell SP, Speed T, Manak JR, Botchan MR (2007). Genomic profiling and expression studies reveal both positive and negative activities for the Drosophila Myb MuvB/dREAM complex in proliferating cells. Genes Dev 21, 2880–2896.

Green RA, Kao HL, Audhya A, Arur S, Mayers JR, Fridolfsson HN, Schulman M, Schloissnig S, Niessen S, Laband K, *et al.* (2011). A high-resolution C. elegans essential gene network based on phenotypic profiling of a complex tissue. Cell 145, 470–482.

Gunsalus KC, Bonaccorsi S, Williams E, Verni F, Gatti M, Goldberg ML (1995). Mutations in twinstar, a Drosophila gene encoding a cofilin/ADF homologue, result in defects in centrosome migration and cytokinesis. J Cell Biol 131, 1243–1259.

Hild M, Beckmann B, Haas SA, Koch B, Solovyev V, Busold C, Fellenberg K, Boutros M, Vingron M, Sauer F, *et al.* (2003). An integrated gene annotation and transcriptional profiling approach towards the full gene content of the Drosophila genome. Genome Biol 5, R3.

Horn T, Boutros M (2013). Design of RNAi reagents for invertebrate model organisms and human disease vectors. Methods Mol Biol 942, 315–346.

Horn T, Sandmann T, Boutros M (2010). Design and evaluation of genome-wide libraries for RNA interference screens. Genome Biol 11, R61.

Horn T, Sandmann T, Fischer B, Axelsson E, Huber W, Boutros M (2011). Mapping of signaling networks through synthetic genetic interaction analysis by RNAi. Nat Methods 8, 341–346.

Jones T, Carpenter A, Golland P (2005). Voronoi-based segmentation of cells on image manifolds. In: Computer Vision for Biomedical Image Applications, ed. Y Liu, T Jiang, and C Zhang, New York: Springer, 535–543.

Jonikas MC, Collins SR, Denic V, Oh E, Quan EM, Schmid V, Weibezahn J, Schwappach B, Walter P, Weissman JS, *et al.* (2009). Comprehensive characterization of genes required for protein folding in the endoplasmic reticulum. Science 323, 1693–1697.

Jorgensen EM, Mango SE (2002). The art and design of genetic screens: Caenorhabditis elegans. Nat Rev Genet 3, 356–369.

Kiger AA, Baum B, Jones S, Jones MR, Coulson A, Echeverri C, Perrimon N (2003). A functional genomic analysis of cell morphology using RNA interference. J Biol 2, 27.

Kittler R, Putz G, Pelletier L, Poser I, Heninger AK, Drechsel D, Fischer S, Konstantinova I, Habermann B, Grabner H, *et al.* (2004). An endoribonuclease-prepared siRNA screen in human cells identifies genes essential for cell division. Nature 432, 1036–1040.

Kondo S, Perrimon N (2011). A genome-wide RNAi screen identifies core components of the G-M DNA damage checkpoint. Sci Signal 4, rs1.

Laufer C, Fischer B, Billmann M, Huber W, Boutros M (2013). Mapping genetic interactions in human cancer cells with RNAi and multiparametric phenotyping. Nat Methods 10, 427–431.

Lehner B, Crombie C, Tischler J, Fortunato A, Fraser AG (2006). Systematic mapping of genetic interactions in Caenorhabditis elegans identifies common modifiers of diverse signaling pathways. Nat Genet 38, 896–903.

Loiodice I, Alves A, Rabut G, Van Overbeek M, Ellenberg J, Sibarita JB, Doye V (2004). The entire Nup107–160 complex, including three new members, is targeted as one entity to kinetochores in mitosis. Mol Biol Cell 15, 3333–3344.

Manley JL (1995). A complex protein assembly catalyzes polyadenylation of mRNA precursors. Curr Opin Genet Dev 5, 222–228.

Morrison AJ, Shen X (2009). Chromatin remodelling beyond transcription: the INO80 and SWR1 complexes. Nat Rev Mol Cell Biol 10, 373–384.

Nurminsky DI, Nurminskaya MV, De Aguiar D, Hartl DL (1998). Selective sweep of a newly evolved sperm-specific gene in Drosophila. Nature 396, 572–575.

Pan X, Yuan DS, Xiang D, Wang X, Sookhai-Mahadeo S, Bader JS, Hieter P, Spencer F, Boeke JD (2004). A robust toolkit for functional profiling of the yeast genome. Mol Cell 16, 487–496.

Patton EE, Zon LI (2001). The art and design of genetic screens: zebrafish. Nat Rev Genet 2, 956–966.

Pau G, Fuchs F, Sklyar O, Boutros M, Huber W (2010). EBImage—an R package for image processing with applications to cellular phenotypes. Bioinformatics 26, 979–981.

Perlman ZE, Mitchison TJ, Mayer TU (2005). High-content screening and profiling of drug activity in an automated centrosome-duplication assay. Chembiochem 6, 145–151.

Rios RM, Sanchis A, Tassin AM, Fedriani C, Bornens M (2004). GMAP-210 recruits gamma-tubulin complexes to cis-Golgi membranes and is required for Golgi ribbon formation. Cell 118, 323–335.
Roguev A, Bandyopadhyay S, Zofall M, Zhang K, Fischer T, Collins SR, Qu H, Shales M, Park HO, Hayles J, *et al*. (2008). Conservation and rewiring of functional modules revealed by an epistasis map in fission yeast. Science 322, 405–410.
Roguev A, Talbot D, Negri GL, Shales M, Cagney G, Bandyopadhyay S, Panning B, Krogan NJ (2013). Quantitative genetic-interaction mapping in mammalian cells. Nat Methods 10, 432–437.
Schmidt EE, Pelz O, Buhlmann S, Kerr G, Horn T, Boutros M (2013). GenomeRNAi: a database for cell-based and in vivo RNAi phenotypes, 2013 update. Nucleic Acids Res 41, D1021–1026.
Schuldiner M, Collins SR, Thompson NJ, Denic V, Bhamidipati A, Punna T, Ihmels J, Andrews B, Boone C, Greenblatt JF, *et al*. (2005). Exploration of the function and organization of the yeast early secretory pathway through an epistatic miniarray profile. Cell 123, 507–519.
Setty SR, Strochlic TI, Tong AH, Boone C, Burd CG (2004). Golgi targeting of ARF-like GTPase Arl3p requires its Nalpha-acetylation and the integral membrane protein Sys1p. Nat Cell Biol 6, 414–419.
Skop AR, Bergmann D, Mohler WA, White JG (2001). Completion of cytokinesis in C. elegans requires a brefeldin A-sensitive membrane accumulation at the cleavage furrow apex. Curr Biol 11, 735–746.
Smyth GK ((2004). Linear models and empirical bayes methods for assessing differential expression in microarray experiments. Stat Appl Genet Mol Biol 3, 1–25.
Somma MP, Fasulo B, Cenci G, Cundari E, Gatti M (2002). Molecular dissection of cytokinesis by RNA interference in Drosophila cultured cells. Mol Biol Cell 13, 2448–2460.
St Johnston D (2002). The art and design of genetic screens: Drosophila melanogaster. Nat Rev Genet 3, 176–188.
Takahashi A, Kikuguchi C, Morita M, Shimodaira T, Tokai-Nishizumi N, Yokoyama K, Ohsugi M, Suzuki T, Yamamoto T (2012). Involvement of CNOT3 in mitotic progression through inhibition of MAD1 expression. Biochem Biophys Res Commun 419, 268–273.
Tanenbaum ME, Stern-Ginossar N, Weissman JS, Vale RD (2015). Regulation of mRNA translation during mitosis. Elife 4, doi: 10.7554/eLife.07957.
Teixido-Travesa N, Roig J, Luders J (2012). The where, when and how of microtubule nucleation—one ring to rule them all. J Cell Sci 125, 4445–4456.
Tischler J, Lehner B, Fraser AG (2008). Evolutionary plasticity of genetic interaction networks. Nat Genet 40, 390–391.
Tong AH, Lesage G, Bader GD, Ding H, Xu H, Xin X, Young J, Berriz GF, Brost RL, Chang M, *et al*. (2004). Global mapping of the yeast genetic interaction network. Science 303, 808–813.
Wang X, Fu AQ, McNerney ME, White KP (2014). Widespread genetic epistasis among cancer genes. Nat Commun 5, 4828.
Zavortink M, Contreras N, Addy T, Bejsovec A, Saint R (2005). Tum/RacGAP50C provides a critical link between anaphase microtubules and the assembly of the contractile ring in Drosophila melanogaster. J Cell Sci 118, 5381–5392.

Supplemental Materials

Molecular Biology of the Cell

Billmann et al.

SUPPLEMENTAL METHODS

Criteria for selection of genes for genetic interaction experiment from genome-wide RNAi screen

To reduce the candidate list to a feasible number of potentially novel cell cycle regulators, several filters were applied. Transcriptomic data from 32 previously conducted RNA sequencing experiments in the same cell line (unpublished data) was used to exclude genes that were not expressed (Reads Per Kilobase per Million mapped reads, RPKM < 5). Further, genes that showed a severe decrease in viability upon knock down (less than 9,000 cells per 384-well, equals >65% reduction compared to control RNAi) were not considered. Using the DRSC Integrative Ortholog Prediction Tool (DIOPT) (Hu *et al.*, 2011) the RNAi library was annotated for human orthologs. Only genes with annotated human ortholog (DIOPT score ≥ 2) were further considered. *Drosophila* genes and their closest human ortholog were functionally annotated using information from FlyBase and Entrez Gene). Genes with functional annotations in cell cycle processes and genes identified in previous cell cycle-related screens in *Drosophila* (Bettencourt-Dias *et al.*, 2004; Bjorklund *et al.*, 2006; Kondo and Perrimon, 2011) were not pursued.

Library of independent reagents for genetic interaction screen

For the genetic interaction experiment two optimized, sequence-independent dsRNAs were designed using NEXT-RNAi (Horn *et al.*, 2010). We aimed at targeting sites independent of the design in the genome-wide library. Further, we defined a fixed length window for the long dsRNAs of 200-225bp and aimed at excluding: (i) perfect 19-nt matches to other than the intended target transcripts, (ii) >6x tandem trinucleotide repeats of the type CA[ACGT] (CAN), (iii) sequence regions of low complexity (e.g. simple nucleotide repeats), (iv) targeting UTRs and overall homology to unintended transcript targets with BLAST E-values $>10^{-10}$. The library was synthesized by a two-step PCR approach followed by *in vitro* transcription(Steinbrink and Boutros, 2008). For dsRNA cleanup, filter plates (MultiScreen HTS PCR 96-Well, Millipore) with columns of Bio-Gel P-30 (Biorad) were prepared. We then measured concentrations using a NanoDrop 1000 spectrophotometer (PEQLAB) and adjusted the concentrations individually for each dsRNA using the Biomek FX Span-8 system. 2.5ul of a 50ng/ul solution (125ng) where then aliquoted into 384-well plates (black/clear, BD Falcon).

Induction of G2/M checkpoint arrest in *Drosophila* S2 cells

To test the mitotic arrest after RNAi for the candidates, 96 h post RNAi induction G2/M checkpoint arrest was triggered for 6 h using 4 µM Doxorubicin or 20 µM Etoposide. With a doubling time of ~30 h and a wild-type mitotic index of <3%, we estimated a duration of the phospho-H3 positive mitosis of ~1 h. Thus, all cell populations in which the RNAi did not result in severe mitotic delay were depleted of phospho-H3 positive cells. Cells were fixed and stained as described for the genome-wide screen. The data was plate-median normalized, log2 transformed and knockdown effects were estimated from two replicates. Z-scores were estimated for the two dsRNA designs to each gene separately.

FACS-based analysis of mitotic exit in human HeLa cells

For knockdown experiments in human HeLa cells, siRNA pools (supplied by Dharmacon, Thermo Scientific) targeting the gene of interest were used. For FACS analysis, a transfection mix containing 1 µl Dharmafect I, 360 µl RPMI and 40 µl siRNAs (250 nM), was prepared. After 30 min incubation at room temperature, 30000 HeLa cells were added in 600 µl DMEM high Glucose medium supplemented with 10% FCS and 1% Penicillin-Streptomycin. Cells were grown for 3 d under standard conditions (37 °C, 5% CO2) and a reversible arrest in prometaphase was induced by incubation with 40 ng/ml nocodazole for 18 h. 0 h, 1 h, 2 h, 3 h, 5 h and 8 h past release from prometaphase by medium exchange, cells were detached by trypsinization and fixed with 70% ethanol over night at -20 °C. Fixed cells were stained for their DNA content in 30 µg/ml propidium iodide (PI) solution (containing 500 µg/ml RnaseA) (Nicoletti *et al.*, 1991) for 30 min at 37 °C. FACS curves were obtained at the FACSDiVa cell sorted and debris and duplet cells were gated in the FSC/SSC scatter blot. To obtain the cell cycle profile, cell count was plotted over PI intensity. The data was analyzed using the FlowJo flow cytometry analysis software.

SUPPLEMENTAL MATERIAL

Figure S1. Correlation of phenotypes from genome-wide RNAi screen. (A) The comparisons of z-scores of two replicates for cell count, nuclear area, and mitotic index show high positive correlations (Pearson). (B) The comparisons of z-scores (of summarized replicates) between the phenotypes show no correlation (Pearson).

Figure S2. Phenotypes of known cell cycle regulators in genome-wide RNAi screen. (A) Fraction of genes per functional group with an absolute z-score ≥ 3 in nuclear area and/or mitotic index phenotypes (see Supplemental Table S3 for the list of genes/functional groups). Colors of processes are matched to groups of scatter plots in B. (B) Scatter plots comparing z-scores for nuclear area and mitotic index (fill color indicates cell count z-score, dashed lines indicate z-score cut-offs of 3 and -3). Genes belonging to different cell cycle processes show differential effects on phenotypes. For example, knockdowns of members of the anaphase-promoting complex/cyclosome (APC/C) show an increased mitotic index with mild to no effects on the nuclear area. Knockdowns of factors important for cytokinesis can affect both, mitotic index and nuclear area (as exemplified in panels C-D). Dashed lines indicate z-scores of 3 and -3. (C) Image crops from screen for knock downs of a negative control (firefly luciferase), the APC/C member *cdc23*, and the cytokinesis regulator *tum*. DNA was stained with Hoechst 33342 (blue), and mitotic cells were labeled by phospho-Histone 3 specific antibody (pink). (D) Quantification of cell count, nuclear area, and mitotic index (n=4 for control, n=2 for cdc23 and tum) for images in C shows that both *cdc23*- and *tum*- knockdowns decrease cell count, but *cdc23* specifically increases mitotic index, while *tum* increases nuclear area.

Figure S3: Quality control and distribution of genetic interactions. (A) Pearson correlation coefficients (PCC) between the interaction profiles across the phenotypes between the two independent dsRNAs used to target each candidate gene. dsRNAs with a PCC below 0.6 (dotted line) were excluded from further analysis. (B) Error distribution of the different phenotypes. Errors were estimated as the difference of the four interaction scores from their mean. Errors between the different phenotypes were adjusted using the mean and the standard deviation of the population of the interaction values. (C-E) Distribution of summarized genetic interactions (π-scores) per

candidate-query gene pair and phenotype. Scores were distributed around '0' and the 25%, 50% and 75% quantiles of the non-targeting (Fluc) dsRNAs are marked as grey lines. (F-H) Distribution of the adjusted p-values for the π-scores per phenotype. P-values were adjusted by using the method by Benjamini and Hochberg.

Figure S4: Transformation of the genetic interaction profile-based association indices. The Relation between the Pearson correlation coefficient (PCC) and the connection specificity index (CSI) in cell count, mitotic index and nuclear area for all quality-selected 350 candidate genes. The curves illustrate that a large fraction of high positive PCCs were corrected for.

Figure S5: Phenotype-specific prioritization of candidate genes. (A) Cell count-based functional association of candidate genes. The tested genes were placed in a force-directed genetic interaction-based network. Only gene pairs with a cell count-based connection specificity index (CSI) > 0.95 were shown. (B, C) Phenotype-specific CSI-based separation of complexes / processes from all tested genes. The distance between genes were estimated by 1 – CSI among the cytokinesis core regulators *Rho1*, *tum*, *lin19* and *zip* (within the complex) (B), or between the APC/C and mitotic spindle components *Arp87C*, *wac*, *dgt2* and *alphaTub84B* (C), and between those genes and all other tested genes (between complex and others). The empirical cumulative distribution functions (ecdf) of the two groups were plotted and the significance of their separation was estimated using a one-sided Wilcoxon rank sum test. (D) FACS profiles of siRNA transfected HeLa cells at different time points past release from Nocodazole-mediated metaphase arrest. Shown is the DNA content of a gated cell population (cell debris removed) for one example replicate. Cell with knockdown of components required for mitotic exit displayed higher fractions of G_2M-resident cell populations after release from metaphase arrest.

Table S1. Target-gene annotation and z-scores for phenotypes from genome-wide RNAi screen.

Table S2. List of knockdowns from genome-wide screen with absolute z-scores ≥ 3 in mitotic index or nuclear area phenotypes, used for heatmap in Figure 2A.

Table S3. Annotation of known cell-cycle regulators for Supplemental Figure S2.

Table S4. Candidate genes and controls selected for genetic interaction analysis (also see Figure S2).

Table S5. Query genes selected for genetic interaction analysis (also see Figure 2F).

Table S6. Genetic interactions between the candidate and query genes for cell count, mitotic index and nuclear area.

Table S7. Connection Specificity Index (CSI) among the candidate genes for cell count, mitotic index and nuclear area.

SUPPLEMENTAL REFERENCES

Bettencourt-Dias, M., Giet, R., Sinka, R., Mazumdar, A., Lock, W.G., Balloux, F., Zafiropoulos, P.J., Yamaguchi, S., Winter, S., Carthew, R.W., Cooper, M., Jones, D., Frenz, L., and Glover, D.M. (2004). Genome-wide survey of protein kinases required for cell cycle progression. Nature *432*, 980-987.

Bjorklund, M., Taipale, M., Varjosalo, M., Saharinen, J., Lahdenpera, J., and Taipale, J. (2006). Identification of pathways regulating cell size and cell-cycle progression by RNAi. Nature *439*, 1009-1013.

Horn, T., Sandmann, T., and Boutros, M. (2010). Design and evaluation of genome-wide libraries for RNA interference screens. Genome Biol *11*, R61.

Hu, Y., Flockhart, I., Vinayagam, A., Bergwitz, C., Berger, B., Perrimon, N., and Mohr, S.E. (2011). An integrative approach to ortholog prediction for disease-focused and other functional studies. BMC Bioinformatics *12*, 357.

Kondo, S., and Perrimon, N. (2011). A genome-wide RNAi screen identifies core components of the G-M DNA damage checkpoint. Sci Signal *4*, rs1.

Nicoletti, I., Migliorati, G., Pagliacci, M.C., Grignani, F., and Riccardi, C. (1991). A rapid and simple method for measuring thymocyte apoptosis by propidium iodide staining and flow cytometry. J Immunol Methods *139*, 271-279.

Steinbrink, S., and Boutros, M. (2008). RNAi screening in cultured Drosophila cells. Methods Mol Biol *420*, 139-153.

A

Comparison of replicates (z-score) per phenotype

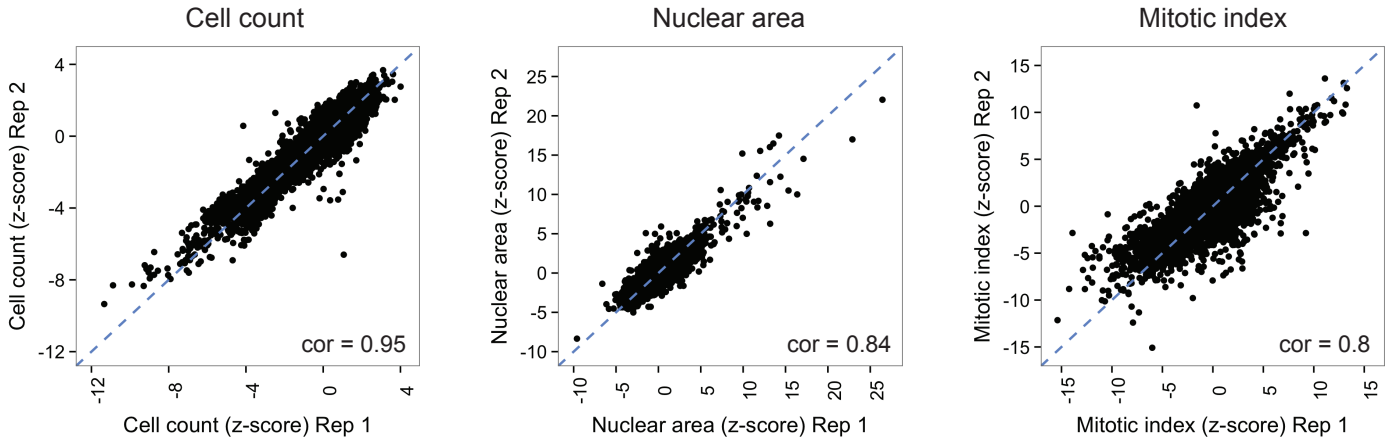

B

Comparison of summarized z-scores between phenotypes

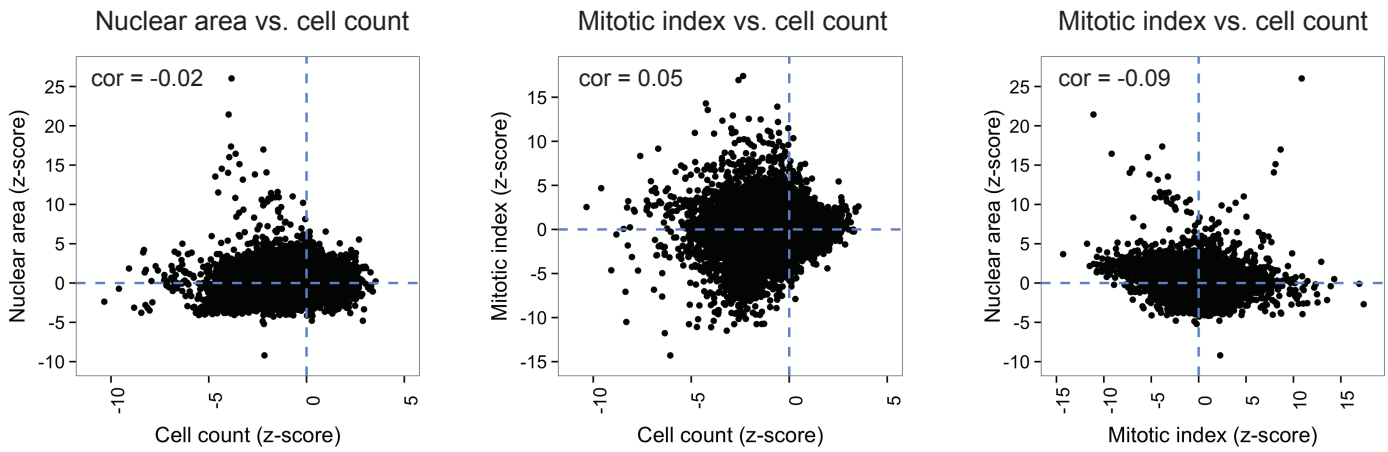

Supplemental Figure 1

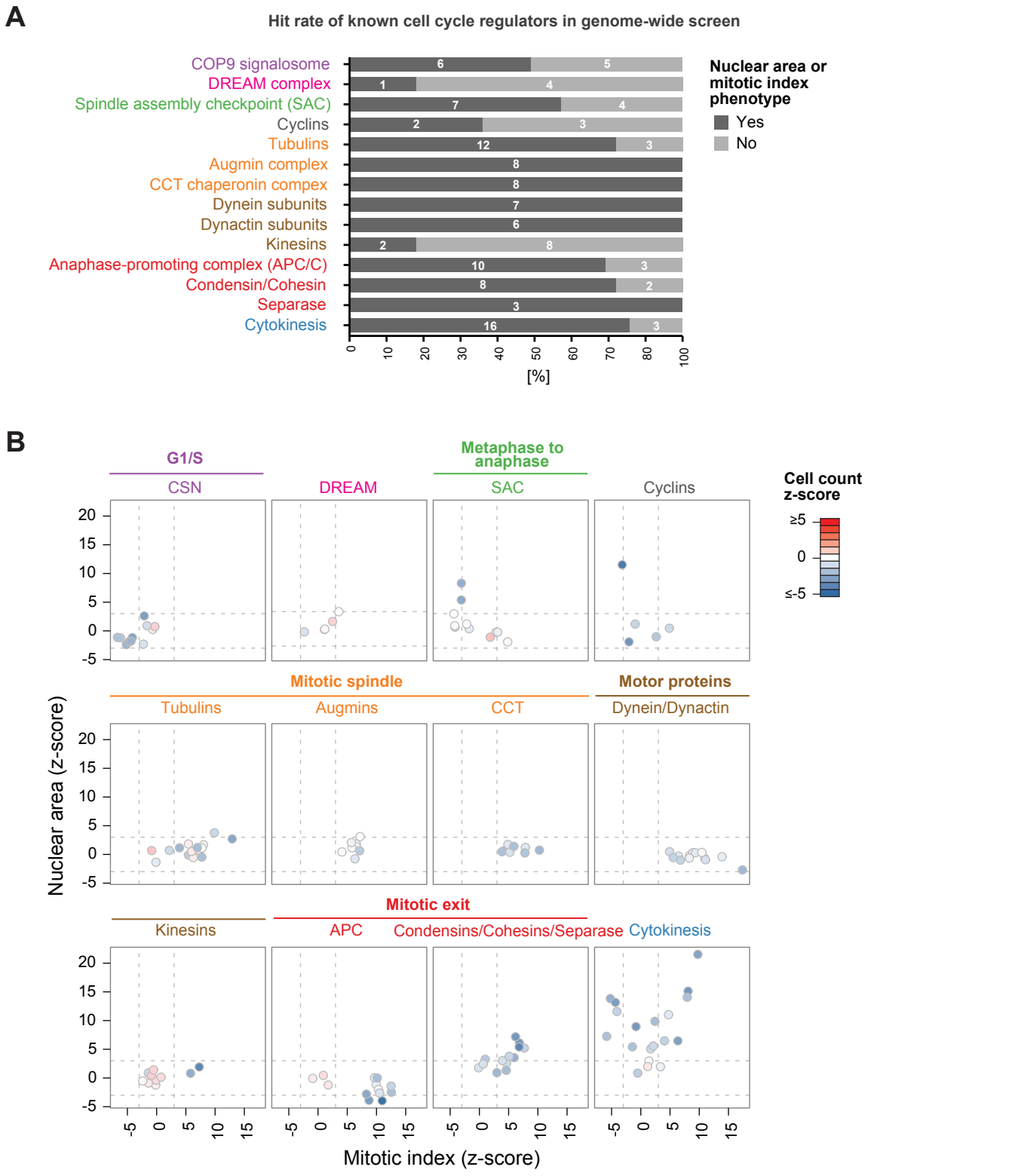

Supplemental Figure 2

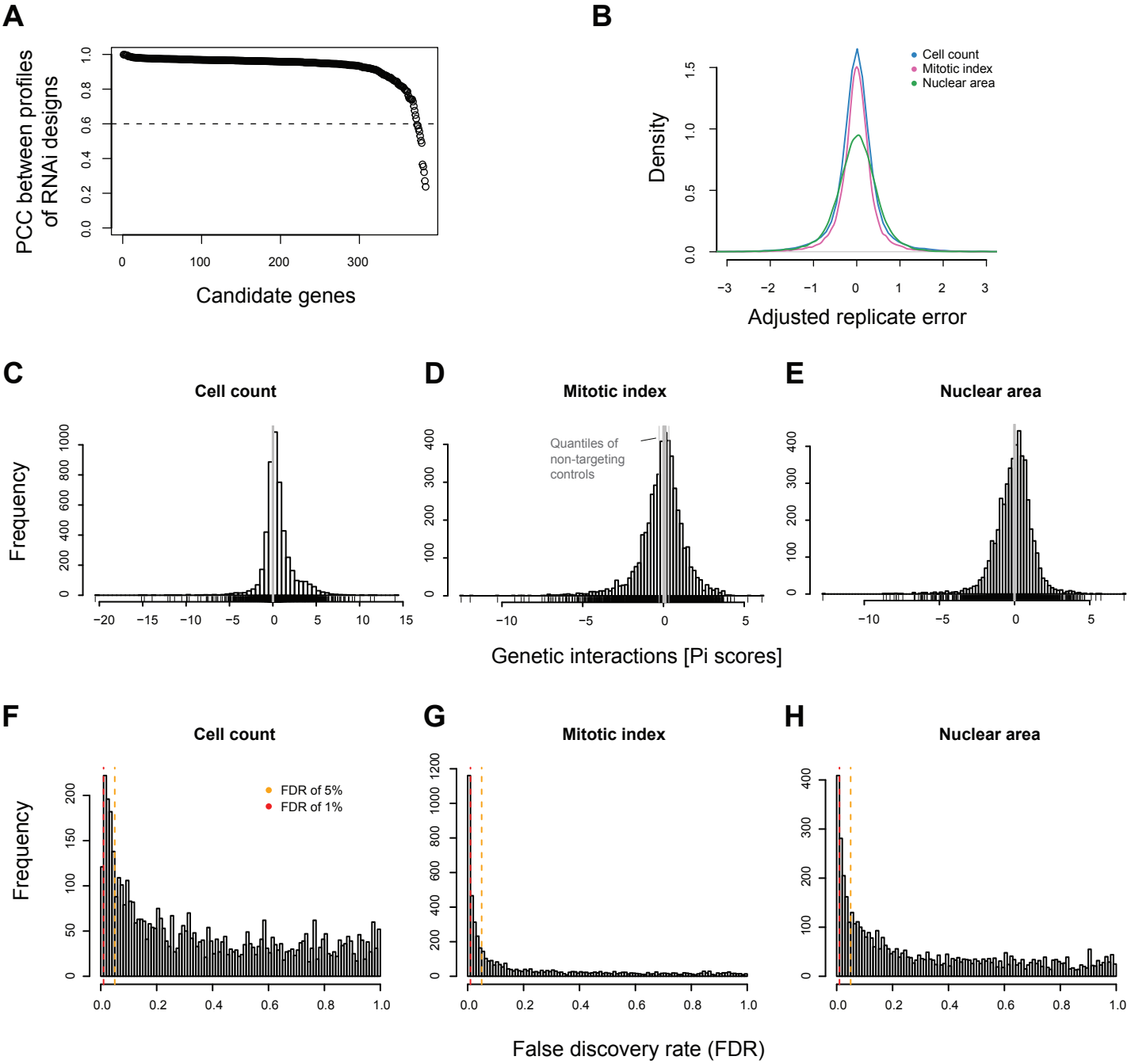

Supplemental Figure 3

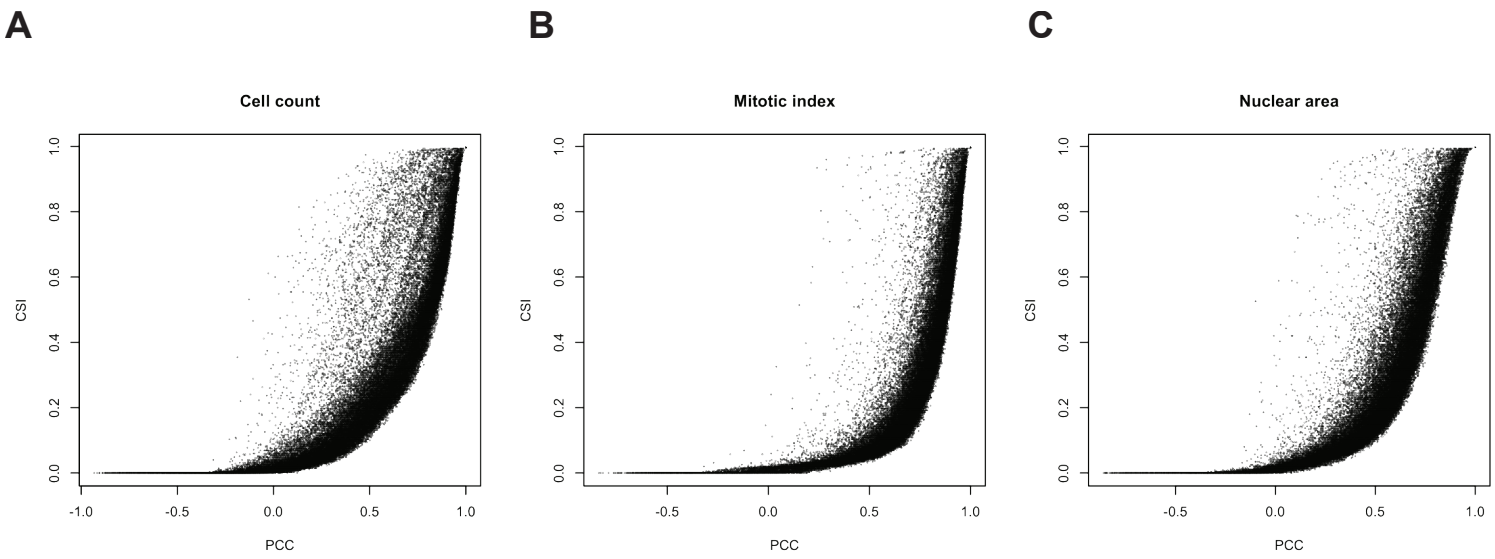

Supplemental Figure 4

Supplemental Figure 5